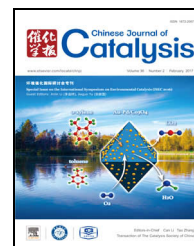


available at www.sciencedirect.comjournal homepage: www.elsevier.com/locate/chnjc

Article (Special Issue on the International Symposium on Environmental Catalysis (ISEC 2016))

Salt-assisted Synthesis of Hollow Bi_2WO_6 Microspheres with Superior Photocatalytic Activity for NO Removal

Meijuan Chen ^a, Yu Huang ^{b,c,*}, Shun Cheng Lee ^d^a School of Human Settlements and Civil Engineering, Xi'an Jiaotong University, Xi'an 710049, Shaanxi, China^b Key Lab of Aerosol Chemistry & Physics, Institute of Earth Environment, Chinese Academy of Sciences, Xi'an 710061, Shaanxi, China^c State Key Lab of Loess and Quaternary Geology (SKLLQG), Institute of Earth Environment, Chinese Academy of Sciences, Xi'an 710061, Shaanxi, China^d Department of Civil and Environmental Engineering, The Hong Kong Polytechnic University, Hung Hom, Hong Kong, China

ARTICLE INFO

Article history:

Received 15 September 2016

Accepted 18 October 2016

Published 5 February 2017

Keywords:

Ultrasonic spray pyrolysis

Salt template

 Bi_2WO_6 hollow microsphere

NO removal

ABSTRACT

Hollow Bi_2WO_6 microspheres are successfully synthesized by a facile ultrasonic spray pyrolysis (USP) method using NaCl as a salt template. The as-prepared hollow microspheres assembled as nanoplates with dimensions of approximately 41–148 nm and are dispersed with non-uniform pores on the template surface. By swapping the salt template with KCl or Na_2SO_4 , different morphologies of Bi_2WO_6 are obtained. The experimental results demonstrate that NaCl plays a key role on the formation of Bi_2WO_6 with hollow structures. The specific growth mechanism of hollow microspheres was studied in detail. The Bi_2WO_6 hollow microspheres exhibit an excellent photocatalytic efficiency for NO removal under solar light irradiation, which is 1.73 times higher than for the Bi_2WO_6 obtained in the absence of any salt template. This enhancement can be ascribed to the simultaneous improvement on the surface area and visible light-harvesting ability from the hollow structures. Electron spin resonance (ESR) results suggest that both radicals of $\bullet\text{OH}$ and $\bullet\text{O}_2^-$ are involved in the photocatalytic process over the BWO-NaCl sample. The production of $\bullet\text{O}_2^-$ radicals offers better durability for NO removal.

© 2016, Dalian Institute of Chemical Physics, Chinese Academy of Sciences.

Published by Elsevier B.V. All rights reserved.

1. Introduction

Nitrogen oxide (NO_x , the sum of NO and NO_2) is one of the main air pollutants emitted from the combustion of fossil fuels [1], which is the most important precursor for the formation of acid rain, photochemical smog and the haze problem in China [2]. The appearance of NO_x in the atmosphere imposes adverse effects on the air quality and human health [3,4]. Therefore, various techniques, including filtration, physical adsorption and thermal catalysis, have been used to remove NO_x from industrial emissions [5,6]. However, the application of most of these

approaches has been hindered because they either need a high temperature to initiate the catalytic conversion reactions or they cause secondary pollution [7]. Hence, novel and practical strategies for reducing the atmospheric NO_x level are an urgent requirement.

Photocatalysis has attracted considerable attention in the past few decades as an effective and promising removal technique for environmental NO_x at ambient temperature [8–10]. Bismuth tungstate (Bi_2WO_6), as one of the simplest compounds in the Aurivillius family ($\text{Bi}_2\text{A}_{n-1}\text{B}_n\text{O}_{3n+1}$; A = Ca, Sr, Ba, Pb, Bi, Na, K and B = Ti, Nb, Ta, Mo, W, Fe), has been reported to exhibit

* Corresponding author. Tel/Fax: +86-29-62336261; E-mail: huangyu@ieecas.cn

This work was supported by the National Natural Science Foundation of China (41503102, 41401567, 41573138); the China Postdoctoral Science Foundation (2015M572568).

DOI: 10.1016/S1872-2067(16)62584-6 | <http://www.sciencedirect.com/science/journal/18722067> | Chin. J. Catal., Vol. 38, No. 2, February 2017

excellent photocatalytic performance under visible light owing to its layered structure and unique catalytic behavior [11]. It is well known that the photocatalytic activity is closely interrelated to the morphology and the size of the photocatalyst [12]. For instance, Bi_2WO_6 can adopt various morphologies, for example, plate [13], particle [14], flower-like [10] and nanocage [12]. It was reported by Wang that the hollow structured Bi_2WO_6 microspheres consist of small nanoparticles (with sizes of 50–80 nm) and exhibit a much better photocatalytic activity than other morphologies, because minimizing the particle size is an effective way to achieve a higher surface area and more active catalytic sites. Moreover, the interconnected nanocrystalline network in hollow spheres shortens the diffusion path of the charge carriers and decreases the resistance from the grain boundaries, and results in the fast mass transfer and high photocatalytic performance [15,16]. Therefore, Bi_2WO_6 with a hollow structure is highly desirable for NO_x removal. The most applied method for the synthesis of Bi_2WO_6 hollow microspheres by far is taking a suitable core as template and growing Bi_2WO_6 colloidal particles on its surface, followed by the removal of the cores by an extra extraction process. Shang et al. [12] synthesized Bi_2WO_6 nanocages using colloidal carbon as the template by a refluxing process in ethylene glycol, followed by calcination to remove the carbon. Homogenous Bi_2WO_6 hollow spheres were synthesized by Sivakumar Natarajan et al. [17] using a silica protected hydrothermal method, after which, the silica-core was etched by the NaOH solvent. Nevertheless, such approaches suffer from the disadvantages of complex synthetic procedures (extra template preparation and removal steps are required) and high cost, which hinders their application.

The ultrasonic spray pyrolysis (USP) method is a versatile technique for preparing nanostructured microspheres with controllable size. To date, the obtained products are typically solid spheres owing to the agglomeration nature of nanocrystals during the decomposition period [18,19]. In previous work, our research group successfully prepared Bi_2WO_6 solid microspheres by the USP method, which presented superior photocatalytic activity owing to their unique morphology [20]. However, the fabrication of hollow Bi_2WO_6 by the USP method has never been reported in a previous study.

Herein, for the first time, we report the fabrication of Bi_2WO_6 hollow microspheres assembled by nanoplates by a simple USP method. The NaCl salt was used as template. The influence of the salt species on the morphologies was investigated. A possible formation mechanism of Bi_2WO_6 hollow microspheres was proposed. The photocatalytic activities of the as-prepared samples were evaluated for NO removal under simulated solar light irradiation. It is demonstrated that the Bi_2WO_6 hollow microspheres show excellent photocatalytic performance.

2. Experimental

2.1. Synthesis of Bi_2WO_6 hollow microspheres

All chemicals were purchased from Sigma-Aldrich and used

as received without further purification. Bismuth tungstate (Bi_2WO_6) microspheres were fabricated by the USP method. In brief, 10 mmol tungstic acid (H_2WO_4) and 20 mmol bismuth citrate ($\text{BiC}_6\text{H}_5\text{O}_7$) were dissolved in concentrated ammonium solution (28% in mass, $\text{NH}_3\cdot\text{H}_2\text{O}$). The obtained two solutions were mixed with magnetic stirring to form a transparent solution. Then, 20 mM salt (NaCl, KCl or Na_2SO_4) solution was added into the above solution to obtain the precursor solution for USP. Finally, the precursor solution was nebulized by an ultrasonic nebulizer at a frequency of $1.7 \text{ MHz} \pm 10\%$ (YUYUE, Shanghai, China). Aerosol droplets generated by the nebulizer were carried into the tubular furnace at a temperature of 873 K by an air gas stream. The products were collected from the percolator located at the furnace outlet, followed by washing several times with ethanol and deionized water. The as-prepared sample obtained by using NaCl salt was abbreviated as BWO-NaCl. For comparison, the samples prepared using KCl and Na_2SO_4 as assisting salts were named as BWO-KCl and BWO- Na_2SO_4 , respectively. The Bi_2WO_6 prepared in the absence of salt was abbreviated as BWO.

2.2. Characterization

The X-ray powder diffraction (XRD) patterns were recorded on a Philips Xpert X-ray diffractometer system with $\text{Cu } K_\alpha$ radiation ($\lambda = 1.54178 \text{ \AA}$) at a scan rate of $2\theta = 0.05^\circ/\text{s}$. The accelerating voltage and the applied current were 40 kV and 30 mA, respectively. The morphology of the obtained samples was characterized by a scanning electron microscope (SEM; JEOL model JSM-6490). A Philips CM-120 electron microscopy instrument was used to record the transmission electron microscopy (TEM) images of the samples. A Varian Cary 100 Scan UV-Visible system equipped with a Labsphere diffuse reflectance accessory was used to obtain the reflectance spectra of the catalysts over a range of 200–800 nm, in which the Labsphere USRS-99-010 was employed as a reflectance standard. X-ray photoelectron spectroscopy (XPS) measurements were performed on a PHI Quantum 2000 XPS System with a monochromatic Al K_α source and a charge neutralizer. All the binding energies were referenced to the C1s peak at 284.8 eV of the surface adventitious carbon. The nitrogen adsorption-desorption isotherms at 77 K were measured using a Micromeritics ASAP 2010 system after the sample was vacuum-dried at 473 K overnight. Samples for electron spin resonance spectroscopy (ESR; ER200-SRC, Bruker, Germany) were prepared by dispersing 0.05 g of photocatalyst into 50 mL of 25 mM 5,5'-dimethyl-1-pyrroline-*N*-oxide (DMPO) solution for DMPO/ $\bullet\text{OH}$ or 50 mL of methanol dispersion for DMPO/ $\bullet\text{O}_2^-$, under irradiation with simulated solar light for 30 s. Measurement conditions of ESR were central field 323.4 mT, modulation frequency 100 kHz, modulation amplitude 0.2 mT, microwave power 3 mW, and temperature 300 K. The microwave frequencies for the hydroxyl radical and superoxide radicals were 9058 and 9074 MHz, respectively.

2.3. Photocatalytic activity test

The photocatalytic activity of the obtained samples was determined by the degradation of NO at ppb levels in a continuous flow reactor under solar light irradiation at ambient temperature (296 ± 1 K). The NO degradation was carried out in a rectangular reactor, which was made of stainless steel with a Saint-Glass window. The volume of the reactor was 4.5 L (30 cm (L) \times 15 cm (W) \times 10 cm (H)). For each test, one sample dish ($d = 12$ cm) containing a well-dispersed Bi_2WO_6 powder was placed in the center of the reactor. The sample dish was prepared by coating an aqueous suspension onto the glass dish, that is, 0.3 g of well-dispersed Bi_2WO_6 suspension was placed onto the glass dish and pretreated at 343 K for several hours until the complete removal of water was achieved. A 300 W commercial tungsten halogen lamp (General Electric) was used as the simulated solar light source. The lamp was placed outside the reactor and the light beam vertically passed through the Saint-Glass window before reaching the sample. The NO gas was acquired from a compressed gas cylinder at a concentration of 48 ppm NO (N_2 balance) with a traceable National Institute of Standards and Technology (NIST) standard. The initial concentration of NO was diluted to approximately 400 ppb by the air stream supplied by a zero air generator (Thermo Environmental Inc. model 111). The humidity level of the NO flow was controlled at 70% by passing the zero air streams through a humidification chamber. The gas streams were premixed completely by a gas blender, and the flow rate was controlled at 3 L/min by a mass flow controller. The lamp was turned on after the adsorption-desorption equilibrium was achieved among water vapor, gases and photocatalysts. The concentration of NO was continuously measured by a chemiluminescence NO analyzer (Thermo Environmental Instruments Inc., model 42c) at a sampling rate of 0.7 L/min.

3. Results and discussion

3.1. Phase structure and morphologies

The structure and composition of the Bi_2WO_6 samples were examined by XRD, as shown in Fig. 1. The distinct diffraction peaks of four BWO samples, including BWO-NaCl, BWO-KCl, BWO-Na₂SO₄ and BWO, were all found at $2\theta = 28.3^\circ, 32.8^\circ, 47.0^\circ, 55.9^\circ, 58.5^\circ$ and 68.9° , which can be indexed to the (131), (200), (202), (133), (262) and (400) planes of orthorhombic Bi_2WO_6 (JCPDS no. 39-0256), respectively, with the lattice constants of $a = 5.456 \text{ \AA}$, $b = 5.436 \text{ \AA}$, and $c = 16.426 \text{ \AA}$. No characteristic peaks of other impurities were observed from the XRD patterns, indicating that pure orthorhombic Bi_2WO_6 could be synthesized by the USP method. This observation suggested that the salt species showed no effect on the structure and composition of the Bi_2WO_6 samples. The average crystallite sizes were calculated using the Scherrer equation [17], where the crystallite size of the BWO, BWO-NaCl, BWO-KCl and BWO-Na₂SO₄ samples were 42.37, 51.81, 46.59 and 58.39 nm, respectively.

The morphologies of the Bi_2WO_6 samples were investigated by SEM and TEM analysis. Fig. 2(a–d) depict the SEM images of BWO, BWO-NaCl, BWO-KCl and BWO-Na₂SO₄, respectively. Fig. 3 shows the TEM images of BWO, and the TEM and HRTEM images of the BWO-NaCl samples. Fig. 2(a) shows that the BWO sample was composed of polydispersed microspheres. Fig. 3(a) and (b) indicate that the BWO sample was comprised of solid microspheres with diameters of approximately 0.5–1.2 μm , and aggregated into small nanoparticles with a diameter of ap-

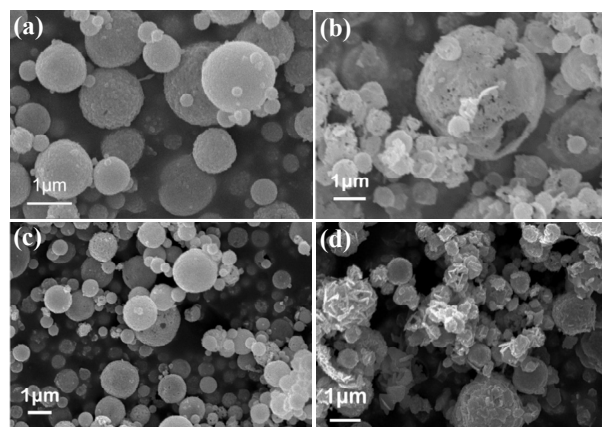


Fig. 2. SEM images of (a) BWO, (b) BWO-NaCl, (c) BWO-KCl and (d) BWO-Na₂SO₄.

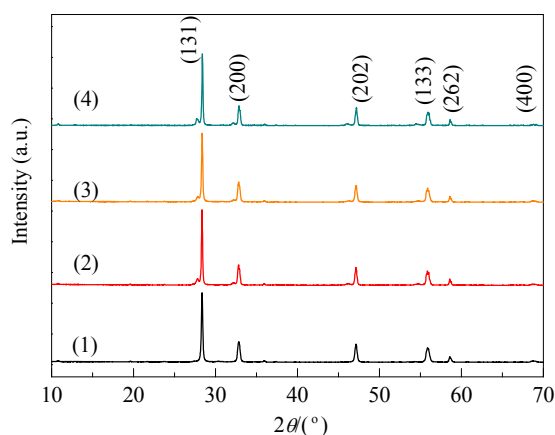


Fig. 1. XRD patterns of the as-prepared (1) BWO, (2) BWO-NaCl, (3) BWO-KCl and (4) BWO-Na₂SO₄ samples.

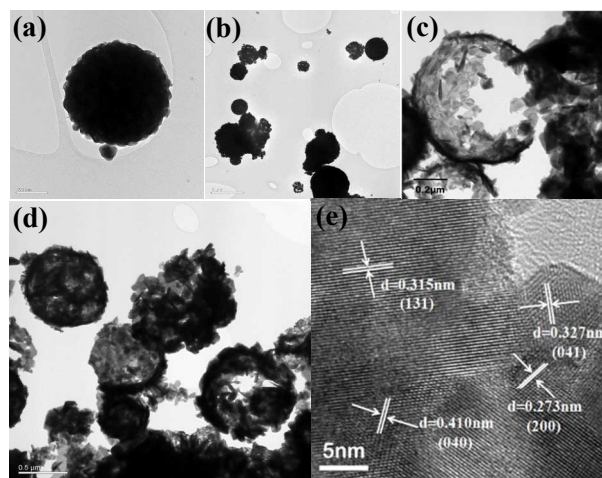


Fig. 3. TEM images of BWO (a, b), BWO-NaCl (c, d), and HRTEM images of the BWO-NaCl sample (e).

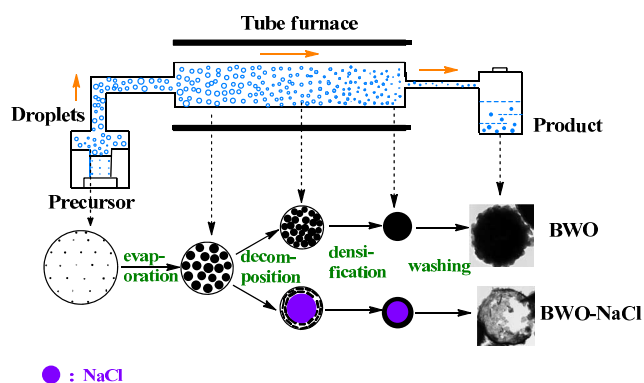
proximately 40 nm. The particle size was in agreement with the calculated result from XRD analysis. From Fig. 2(b), non-uniform large cavities and small pores were observed on the BWO-NaCl surface. The structure was further investigated by TEM spectroscopy. As shown in Fig. 3(c), the BWO-NaCl presented a shell-like hollow microspheres structure. In agreement with the SEM images, the large cavities and small pores were also found on the surface. The diameters of the hollow microspheres ranged from 1.0 to 2.3 μm (see Fig. 3(d)), which is much larger than those of BWO. This is proposed to be because the NaCl can enlarge the droplets formed in the earlier stage of USP. A similar phenomenon was revealed in a previous study, where the $\text{Y}_2\text{O}_3\text{-ZrO}_2$ microspheres obtained from salt-assisted USP method showed a bigger size than those without salt addition [21]. Moreover, the hollow BWO-NaCl were comprised into nanoplates with dimensions of 41.2–148.4 nm, rather than nanoparticles as obtained in the BWO sample.

To specify the role of NaCl, the effect of Cl^- and Na^+ ions were investigated by using KCl and Na_2SO_4 as precursors, respectively. In general, the presence of KCl and/or Na_2SO_4 both had a significant influence on the Bi_2WO_6 morphology. In Fig. 2(c), the BWO-KCl consisted of polydispersed microspheres dispersed with small pores on the surface. In agreement with the morphology of BWO-NaCl, the formation of small pores on the Bi_2WO_6 surface should be ascribed to the presence of the Cl^- ion. Fig. 2(d) reveals that the microspheres in BWO- Na_2SO_4 were aggregated into nanoplates, indicating Na^+ ion played a key role for fabricating the nanoplates [22].

The high-resolution TEM (HRTEM) image of BWO-NaCl was recorded at the edge of an individual microsphere. As shown in Fig. 3(e), the fringe spacing at approximately 0.273, 0.315, 0.327 and 0.410 nm correspond to the lattice spacings of the (200), (131), (041) and (040) planes of orthorhombic Bi_2WO_6 , respectively [23]. The phase analysis from HRTEM confirmed the orthorhombic phase structure analyzed from XRD.

3.2. Formation mechanism of the hollow structured Bi_2WO_6 microspheres

It is known that the aerosol-assisted USP method commonly proceeds in several stages, that is, droplet generation, solvent evaporation, solute diffusion, precipitation, decomposition, and densification [24]. The formation process of a solid BWO microsphere has been demonstrated in our previous study [20]. Briefly, when the nebulized droplets carrying solutes of ammonium bismuth citrate and ammonium paratungstate (formed in the ammonia solution) undergo high temperature treatment, solvent evaporation and solute diffusion occurs. The decomposed products react with each other and produce crystallized Bi_2WO_6 particles, which are then assembled into a solid sphere through free aggregation (see Scheme 1). On the basis of the experiments and characterizations, the formation of the hollow BWO-NaCl microspheres was proposed as follows. First, when the droplets pass through the furnace at high temperature, a single NaCl crystal is obtained by the calcination step, which can act as the core template and is surrounded by a chemical



Scheme 1. The formation mechanism of hollow Bi_2WO_6 microspheres.

shell (ammonium bismuth citrate and ammonium paratungstate). This observation has been proven by Brinker and co-worker [25] in the synthesis of hollow silica microspheres by the NaCl-assisted USP process. Second, the Bi_2WO_6 nanoplates grow on the surface of the NaCl crystal by a chemical reaction between ammonium bismuth citrate and ammonium paratungstate. It should be noted that the Na^+ ion assists in the growth of the nanoplates. Simultaneously, the volatile gases of NH_3 and CO_x ($\text{CO}_2 + \text{CO}$) escaped from the shell to leave pores, where the volatile gases of NH_3 and CO_x were produced from the decomposition of ammonium and citrate, respectively. In addition, the Cl^- ion also contributed to the small pores, as observed from the SEM characterization. Finally, the NaCl crystal leaching in the washing step resulted in the formation of the hollow microspheres. Besides, the NaCl crystal also acted as the porosity inducing agent [26], which produced pores after it leached out and consequently increased the porosity of the final prepared BWO-NaCl.

3.3. Surface compositions of hollow Bi_2WO_6 microspheres

X-ray photoelectron spectroscopy (XPS) was used to characterize the surface compositions and chemical state of the as-prepared hollow BWO-NaCl microspheres. Fig. 4 shows the high-resolution spectra of C1s, Bi 4f, W 4f and O1s of BWO-NaCl. The C1s peak was ascribed to the surface adventitious carbon (Fig. 4(a)). In Fig. 4(b), the two Bi 4f peaks with binding energies at 158.3 and 163.6 eV, corresponding to Bi 4f_{7/2} and Bi 4f_{5/2}, respectively, were attributed to the trivalent oxidation state of Bi [20]. The peaks appearing at binding energies of 36.8 and 34.8 eV in Fig. 4(c) were assigned to the W^{6+} oxidation state [27]. The O 1s XPS spectra peak with a binding energy of 529.7 eV corresponded to the oxygen species in the orthorhombic Bi_2WO_6 phase [27]. The peak observed close to 531.9 eV in the O1s spectra indicated the presence of a hydroxyl (-OH) species adsorbed on the Bi_2WO_6 surface [28].

3.4. Optical properties

UV-vis diffuse reflectance spectroscopy (DRS) was performed to characterize the light absorption properties of the as-prepared Bi_2WO_6 samples. As shown in Fig. 5, the absorption

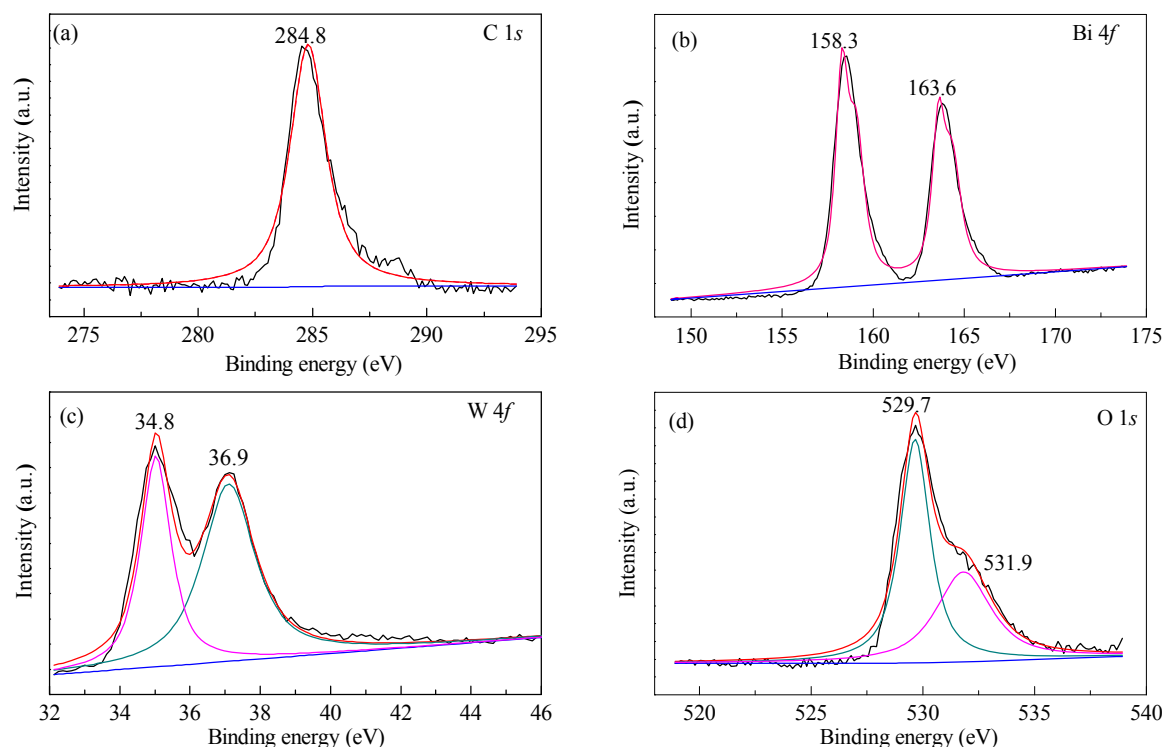


Fig. 4. XPS profiles spectra of hollow BWO-NaCl microspheres (a) C1s, (b) Bi 4f, (c) W 4f, and (d) O1s.

spectrum of BWO extends from the UV region to the visible region at 450 nm. Compared with BWO, the BWO-NaCl spectrum showed a slight red-shift of the absorption edge and displayed an improved absorption around 450–600 nm. This observation clearly indicated that BWO-NaCl exhibited a stronger absorption within the visible light range, which should be an advantage for a better photocatalytic activity owing to its enhanced light-harvesting ability. The band gap of Bi_2WO_6 samples can be estimated according to the Kubelka-Munk function [29]:

$$\alpha h\nu = A(h\nu - E_g)^{n/2}$$

where α , h , ν and E_g are the absorption coefficient, constant, light frequency and band-gap energy, respectively. It is known that $n = 1$ by assuming Bi_2WO_6 to be a direct semiconductor. The E_g of BWO, BWO-NaCl, BWO-KCl and BWO- Na_2SO_4 were estimated to be 2.58, 2.56, 2.54 and 2.51 eV, respectively, by plotting the $(\alpha h\nu)^2$ versus photon energy $h\nu$ (see inset of Fig. 5). These results indicate that all Bi_2WO_6 samples showed a suitable E_g for photocatalytic reaction under visible light irradiation. Moreover, all the salt-assisted Bi_2WO_6 samples, including BWO-NaCl, BWO-KCl and BWO- Na_2SO_4 , exhibited better visible light absorption than BWO. It was reported by He and co-workers [30] that the morphologies of Bi_2WO_6 significantly affect the light absorption property, where the Bi_2WO_6 nanoplates showed a smaller E_g than nanoparticles. Our results are in agreement with their finding that the E_g of Bi_2WO_6 microspheres composed of nanoplates (i.e., BWO-NaCl and BWO- Na_2SO_4) was lower than those of nanoparticles (i.e., BWO-KCl and BWO). Moreover, in contrast to the light only arriving at the outside surface of solid BWO spheres, in the BWO-NaCl sample, the light reached the interior of the hollow

spheres followed by multiple reflections in the hollow space, which allowed an efficient use of light energy and improved the photocatalytic activity [15].

3.5. BET test

The N_2 adsorption-desorption isotherms and pore size distribution curves of BWO and BWO-NaCl samples are shown in Fig. 6. Both samples can be classified as type IV in the IUPAC classification with a distinct hysteresis loop observed in the range of $p/p_0 = 0.4$ –1.0, which are characteristic of porous materials. The Brunauer-Emmett-Teller (BET) specific surface area of the BWO-NaCl sample was approximately $11.2 \text{ m}^2/\text{g}$. It

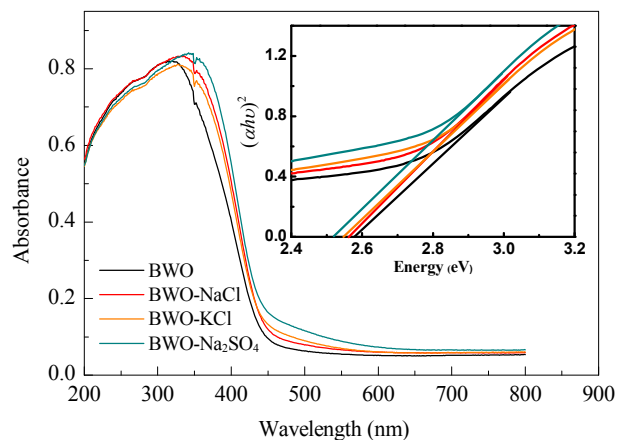


Fig. 5. UV-vis absorption spectroscopy of the as-prepared samples of BWO, BWO-NaCl, BWO-KCl and BWO- Na_2SO_4 . The inset is a plot of $(\alpha h\nu)^2$ versus photon energy ($h\nu$), where α is the absorption coefficient.

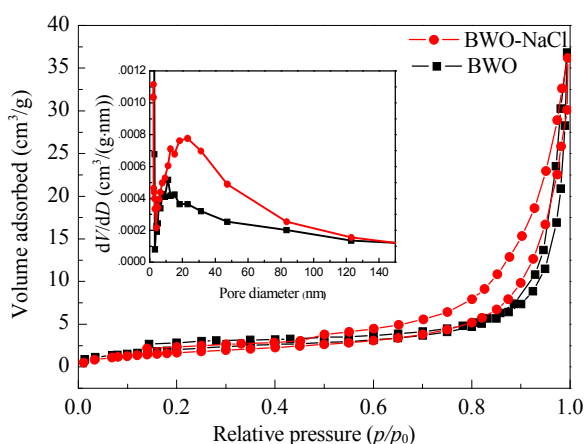


Fig. 6. N_2 adsorption and desorption isotherms and pore-size distribution (inset) of BWO-NaCl and BWO.

was bigger than the BWO sample, as its specific surface area was $9.7 \text{ m}^2/\text{g}$. It can be deduced that the use of NaCl in the precursor could increase the specific surface area of the sample. This improvement takes advantage of the absorption of more active species and pollutant molecules on its surface, and consequently favors the photocatalytic activity. The Barrett-Joyner-Halenda (BJH) pore-size distribution plot for the N_2 sorption isothermal is shown in the inset of Fig. 6. The pore size distribution curve of BWO-NaCl displayed a unimodal type of pores with a mean diameter of approximately 30 nm, when the BWO sample showed a mean diameter of 18 nm.

3.6. Photocatalytic activity of NO removal

To investigate the morphology-dependent photocatalytic activity of the as-synthesized Bi_2WO_6 microspheres, the air pollutant NO was used as the photoreaction probe at an initial NO concentration of 400 ppb. Fig. 7(a) displays the relative NO removal efficiency against irradiation time under the irradiation of simulated solar light. Among the four Bi_2WO_6 samples, the NO removal efficiency over the BWO-NaCl sample reached the highest value of 44.5%. The BWO, BWO-KCl and

BWO- Na_2SO_4 samples possessed a NO removal efficiency of 25.7%, 30.0% and 36.9%, respectively, demonstrating the salt species significantly affect the photocatalytic activity of Bi_2WO_6 . For a clear quantitative comparison, the Langmuir-Hinshelwood model was used to describe the initial rates for NO degradation [10]. The initial NO removal (in the first 3 min) was found to follow pseudo-first-order kinetics as evidenced by the linear plot of $\ln(c/c_0)$ versus reaction time (Fig. 7(b)). The initial rate constant (k , min^{-1}) of BWO-NaCl was estimated as 0.181 min^{-1} , faster than those of BWO (0.068 min^{-1}), BWO-KCl (0.088 min^{-1}) and BWO- Na_2SO_4 (0.159 min^{-1}). It was noted that the BET surface area of BWO-NaCl ($11.2 \text{ m}^2/\text{g}$) was higher than that of BWO ($9.7 \text{ m}^2/\text{g}$), illustrating that the higher surface area of Bi_2WO_6 was a key factor for the higher initial rate constant and higher NO removal rate. This arises because a large specific surface area can supply abundant unsaturated sites on the catalyst surface, accelerating the diffusive transport of photogenerated holes to oxidizable species [31]. However, the difference in pore size of Bi_2WO_6 has been believed to be another key factor for the difference in photocatalytic performance in the literature [32], where the bigger average pore size of Bi_2WO_6 resulted in a better photocatalytic performance. Similarly, in this study, the BWO-NaCl with an average pore size of 30 nm showed a better performance than BWO with an average pore size of 18 nm. This is because the suitable pore size allowed light waves to penetrate deep inside the microsphere and led to a high mobility of charge carriers [33]. Meanwhile, the suitable pore size offered a quick transformation channel for the pollutant and sped up the pollutant degradation [34]. Overall, these results illustrate that the nanoplates-comprised porous BWO-NaCl catalyst with hollow microsphere morphologies was superior to ensure a rapid and high degree of NO removal. Fig. 7(c) shows the NO_2 accumulation profile by BWO-NaCl under simulated solar light. It can be observed that nearly 25% of decontaminated NO is transferred to NO_2 .

3.7. Insights into the photocatalytic degradation mechanism of NO

To clarify the reaction mechanism of the photocatalytic oxi-

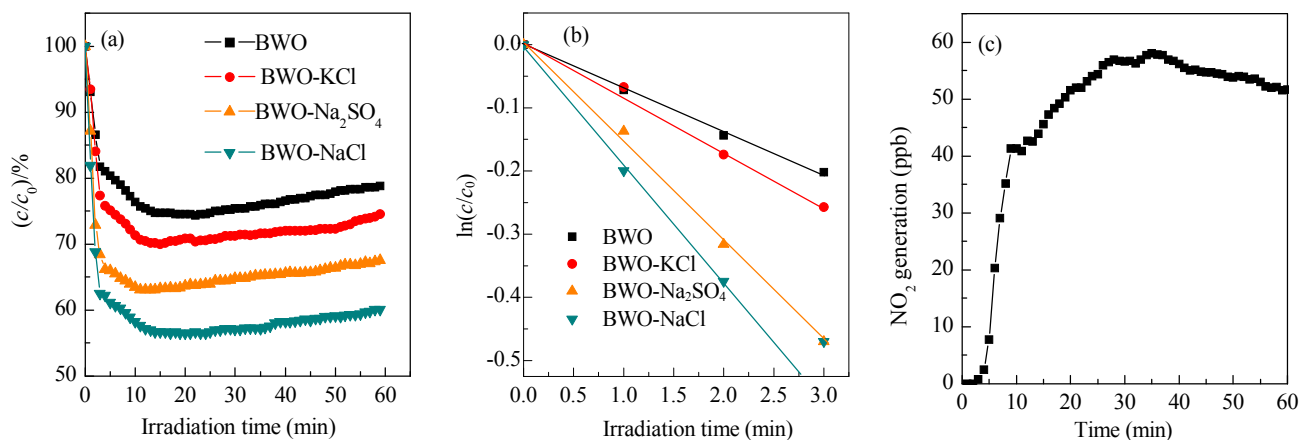
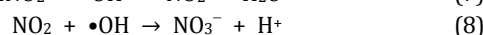
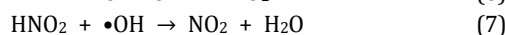
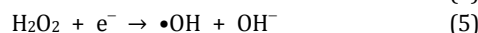
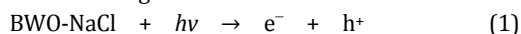


Fig. 7. (a) NO degradation curves, (b) the pseudo-first-order kinetics for NO degradation under simulated solar light irradiation and (c) the accumulation profile of NO_2 by BWO-NaCl under simulated solar light.

dation of NO over Bi₂WO₆ samples, the ESR spin-trap technique was performed to probe the active oxygen species during the photocatalytic processes. Fig. 8 showed the ESR spectra obtained using DMPO as the spin-trap reagent under simulated solar light irradiation. No ESR signal was observed when the tests were performed with Bi₂WO₆ samples in the dark. The 7-line characteristic peaks in Fig. 8(a) indicate that both BWO and BWO-NaCl produced considerable hydroxyl radicals by solar light photocatalysis [35]. The 7-line characteristic peaks should be ascribed to the di-substituted adducts of DMPO (DMPOX, 5,5-dimethyl-2-pyrrolidone-*N*-oxyl), rather than the four-line ESR signal of DMPO-OH (5,5-dimethyl-2-hydroxypyrrolidine-*N*-oxyl) [36]. This is because the abundant hydroxyl radicals generated from BWO-NaCl photocatalysis lead to the DMPO-OH oxidizing to DMPOX intermediately without any residue [37]. This observation demonstrated that our synthesized BWO-NaCl and BWO were powerful catalysts for generating hydroxyl radicals [37].

The 4-line spectrum of BWO-NaCl in Fig. 8(b) displays a characteristic intensity of 1:1:1:1 originating from the DMPO/•O₂⁻ adduct, suggesting the •O₂⁻ radicals were produced during the BWO-NaCl photocatalysis process [38]. In contrast, a 6-line ESR spectrum was obtained in the BWO sample. This spin adduct could be characterized as the methoxyl spin adduct of DMPO, that is DMPO/•CH₂OH. The signal for the DMPO/•CH₂OH adduct originates from the attack of •OH radicals [39]. The interaction of •OH radicals and methanol ultimately leads to the loss of a hydrogen atom from the CH₃ group in methanol and the formation of the DMPO/CH₂OH adduct [40]. In addition, the presence of the DMPO/•O₂⁻ adduct signals and the absence of the DMPO/CH₂OH signal in the BWO-NaCl photocatalyst could be explained by the formation of DMPO/CH₂OH being suppressed in the presence of superoxide [39].

In general, the photocatalytic performance of the semiconductor was highly dependent on its morphology, light absorption, surface area and the active oxygen species. Based on above analysis, the NO degradation mechanism on BWO-NaCl was proposed as following:



First, the •OH and •O₂⁻ radicals were produced during the BWO-NaCl photocatalysis process (Eqs. 1–5). After which, the generated active species of •OH react with NO to generate NO₃⁻ (Eqs. 6–8). The yield of NO₂ by-product in Eq. 7 was proven by the detection of NO₂ during the photocatalytic reaction (see Fig. 7c). It should be noted that the •O₂⁻ radicals generated from BWO-NaCl can be further reduced to •OH radicals (Eqs. 4–5), which would assist in the NO abatement by integrating Eqs. 3–8 into one new pathway (Eq. 9):



It can be seen that the •O₂⁻ radicals can transfer NO into NO₃⁻ without producing H⁺ ions. Therefore, the drawback (i.e., deactivation in NO removal curves) of a pH decrease will be hindered in the •O₂⁻ induced degradation process. Therefore, the BWO-NaCl sample should possess better durability for NO removal owing to the production of •O₂⁻ radicals.

Recycling experiments were conducted to test the stability of the optimum photocatalyst of the BWO-NaCl sample. As shown in Fig. 9, the NO removal efficiency in the five consecutive cycles was (100, 96.3, 89.7, 96.4, 87.9 and 87.3)%, respectively. Hence, a high performance after recycling was maintained, suggesting the obtained BWO-NaCl photocatalyst possesses high stability and no photocorrosion occurs during the NO decay period.

4. Conclusions

In this study, hollow structured Bi₂WO₆ microspheres composed of nanoplates were synthesized by a facile USP method with the assistance of NaCl salt. The BWO-NaCl showed a broadening in the absorption range and higher specific surface area compared with the bulk BWO sample. The NaCl crystal acted as a core for the formation of the hollow structure of Bi₂WO₆ microspheres. Moreover, Na⁺ served as the template for nanoplates, and Cl⁻ contributed to the small pores on the

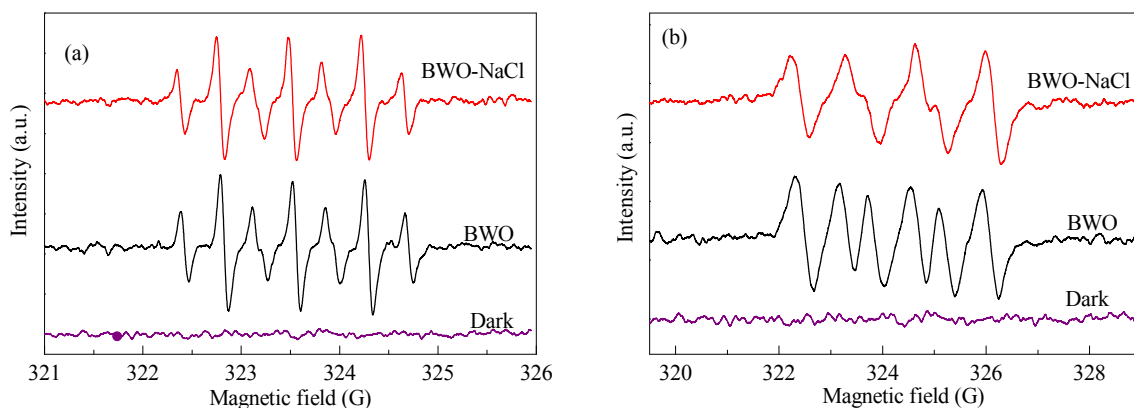


Fig. 8. ESR spectra tests for the detection of (a) •OH in aqueous solution and (b) •O₂⁻ in methanol solvent.

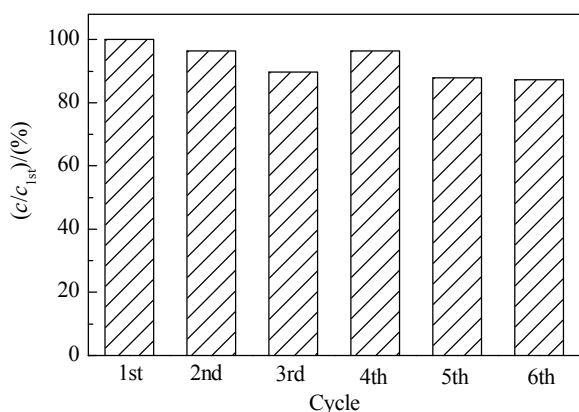


Fig. 9. Cycling tests for NO removal by the BWO-NaCl photocatalyst under simulated solar light irradiation. The BWO-NaCl was washed by DI water before being reused.

surface. As a result, the hollow BWO-NaCl possessed excellent solar light photocatalytic performance for NO with a removal rate of 43.5%, which is 1.69, 1.45 and 1.04 times greater than those of BWO, BWO-KCl and BWO-Na₂SO₄, respectively. Additionally, the initial rate constant of BWO-NaCl was estimated to be 0.181 min⁻¹, which is faster than those of BWO (0.068 min⁻¹), BWO-KCl (0.088 min⁻¹) and BWO-Na₂SO₄ (0.159 min⁻¹). These observations suggest that the salts species have an important effect on the photocatalytic activity of Bi₂WO₆. The main oxidative species were confirmed as •OH and •O₂⁻ radicals in the BWO-NaCl photocatalysis, based on which, an enhanced mechanism was proposed accordingly, where the •O₂⁻ radicals contributed to the better durability of BWO-NaCl for NO removal.

References

- [1] A. Farrell, *Energy Policy*, **2001**, 29, 1061–1072.
- [2] R. J. Huang, Y. L. Zhang, C. Bozzetti, K. F. Ho, J. J. Cao, Y. M. Han, K. R. Daellenbach, J. G. Slowik, S. M. Platt, F. Canonaco, P. Zotter, R. Wolf, S. M. Pieber, E. A. Brunns, M. Crippa, G. Ciarelli, A. Piazzalunga, M. Schwikowski, G. Abbaszade, J. Schnelle-Kreis, R. Zimmermann, Z. S. An, S. Szidat, U. Baltensperger, I. El Haddad, A. S. H. Prevot, *Nature*, **2014**, 514, 218–222.
- [3] C. H. Ao, S. C. Lee, C. L. Mak, L. Y. Chan, *Appl. Catal. B*, **2003**, 42, 119–129.
- [4] T. L. Wu, X. X. Li, D. K. Zhang, F. Dong, S. J. Chen, *J. Alloys Compd.*, **2016**, 671, 318–327.
- [5] L. Giraldo, J. C. Moreno-Pirajan, *J. Therm. Anal. Calorim.*, **2015**, 121, 245–255.
- [6] M. K. Camarillo, W. T. Stringfellow, J. S. Hanlon, K. A. Watson, *Appl. Energy*, **2013**, 106, 328–336.
- [7] R. T. Guo, J. K. Hao, W. G. Pan, Y. L. Yu, *Sep. Sci. Technol.*, **2015**, 50, 310–321.
- [8] Z. H. Ai, W. Ho, S. Lee, L. Z. Zhang, *Environ. Sci. Technol.*, **2009**, 43, 4143–4150.
- [9] J. Lasek, Y. H. Yu, J. C. S. Wu, *J. Photochem. Photobiol. C*, **2013**, 14, 29–52.
- [10] G. S. Li, D. Q. Zhang, J. C. Yu, M. K. H. Leung, *Environ. Sci. Technol.*, **2010**, 44, 4276–4281.
- [11] L. S. Zhang, H. L. Wang, Z. G. Chen, P. K. Wong, J. S. Liu, *Appl. Catal. B*, **2011**, 106, 1–13.
- [12] M. Shang, W. Z. Wang, H. L. Xu, *Cryst. Growth Des.*, **2009**, 9, 991–996.
- [13] M. Shang, W. Z. Wang, S. M. Sun, L. Zhou, L. Zhang, *J. Phys. Chem. C*, **2008**, 112, 10407–10411.
- [14] C. X. Xu, X. Wei, Z. H. Ren, Y. Wang, G. Xu, G. Shen, G. R. Han, *Mater. Lett.*, **2009**, 63, 2194–2197.
- [15] F. Dong, Y. Huang, S. C. Zou, J. Liu, S. C. Lee, *J. Phys. Chem. C*, **2011**, 115, 241–247.
- [16] X. J. Wang, X. L. Wan, L. L. Chang, *Mater. Lett.*, **2014**, 144, 1268–1277.
- [17] T. Sivakumar, Natarajan, H. C. Bajaj, R. J. Tayade, *CrystEngComm*, **2015**, 17, 1037–1049.
- [18] Y. Huang, K. J. Deng, Z. H. Ai, L. Z. Zhang, *Mater. Chem. Phys.*, **2009**, 114, 235–241.
- [19] Y. Huang, Z. Zheng, Z. H. Ai, L. Z. Zhang, X. X. Fan, Z. G. Zou, *J. Phys. Chem. B*, **2006**, 110, 19323–19328.
- [20] Y. Huang, Z. H. Ai, W. Ho, M. J. Chen, S. Lee, *J. Phys. Chem. C*, **2010**, 114, 6342–6349.
- [21] B. Xia, I. W. Lenggoro, K. Okuyama, *Adv. Mater.*, **2001**, 13, 1579–1582.
- [22] T. H. Zheng, J. B. Pang, G. Tan, J. B. He, G. L. McPherson, Y. F. Lu, V. T. John, J. J. Zhan, *Langmuir*, **2007**, 23, 5143–5147.
- [23] J. Di, J. X. Xia, Y. P. Ge, H. P. Li, H. Y. Ji, H. Xu, Q. Zhang, H. M. Li, M. N. Li, *Appl. Catal. B*, **2015**, 168–169, 51–61.
- [24] J. H. Bang, K. S. Suslick, *Adv. Mater.*, **2010**, 22, 1039–1059.
- [25] X. Jiang, C. J. Brinker, *J. Am. Chem. Soc.*, **2006**, 128, 4512–4513.

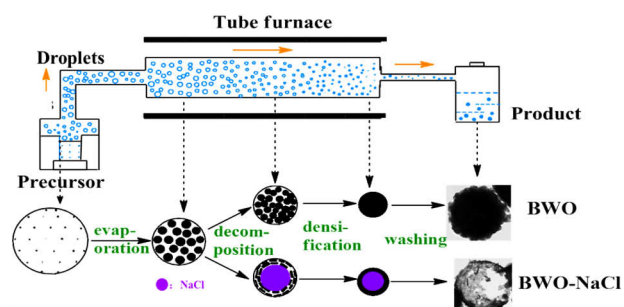
Graphical Abstract

Chin. J. Catal., 2017, 38: 348–356 doi: 10.1016/S1872-2067(16)62584-6

Salt-assisted Synthesis of Hollow Bi₂WO₆ Microspheres with Superior Photocatalytic Activity for NO Removal

Meijuan Chen, Yu Huang*, Shun Cheng Lee
Xi'an Jiaotong University; Institute of Earth Environment, Chinese Academy of Sciences; The Hong Kong Polytechnic University

Hollow Bi₂WO₆ microspheres are successfully synthesized by a facile ultrasonic spray pyrolysis (USP) method with NaCl as the salt template. Excellent photocatalytic efficiency for NO removal under solar light irradiation is achieved.



- [26] D. Chen, G. Wang, H. Zhang, J. H. Li, *J. Nanosci. Nanotechnol.*, **2009**, 9, 2456–2462.
- [27] J. H. Ryu, S. Y. Bang, W. S. Kim, G. S. Park, K. M. Kim, J. W. Yoon, K. B. Shim, N. Koshizaki, *J. Alloys Compd.*, **2007**, 441, 146–151.
- [28] B. Varghese, T. C. Hoong, Y. W. Zhu, M. V. Reddy, B. V. R. Chowdari, A. T. S. Wee, T. B. C. Vincent, C. T. Lim, C. H. Sow, *Adv. Funct. Mater.*, **2007**, 17, 1932–1939.
- [29] P. Madhusudan, J. G. Yu, W. G. Wang, B. Cheng, G. Liu, *Dalton Trans.*, **2012**, 41, 14345–14353.
- [30] Z. He, C. Sun, S. G. Yang, Y. C. Ding, H. He, Z. L. Wang, *J. Hazard. Mater.*, **2009**, 162 1477C1486.
- [31] S. Choudhary, S. Upadhyay, P. Kumar, N. Singh, V. R. Satsangi, R. Shrivastav, S. Dass, *Int. J. Hydrogen Energy*, **2012**, 37, 18713–18730.
- [32] Y. W. Mi, S. Y. Zeng, L. Li, Q. F. Zhang, S. N. Wang, C. H. Liu, D. Z. Sun, *Mater. Res. Bull.*, **2012**, 47, 2623–2630.
- [33] X. C. Wang, J. C. Yu, C. M. Ho, Y. D. Hou, X. Z. Fu, *Langmuir*, **2005**, 21, 2552–2559.
- [34] C. S. Guo, M. Ge, L. Liu, G. D. Gao, Y. C. Feng, Y. Q. Wang, *Environ. Sci. Technol.*, **2010**, 44, 419–425.
- [35] Y. S. Wang, J. H. Shen, J. J. Horng, *Biomed. Eng. Biotechnol.*, **2012**, International Conference on Macau, 1881–1884.
- [36] W. W. He, Y. T. Liu, W. G. Wamer, J. J. Yin, *J. Food Drug Anal.*, **2014**, 22, 49–63.
- [37] J. Kuncewicz, P. Zabek, K. Kruczala, K. Szacilowski, W. Macyk, *J. Phy. Chem. C*, **2012**, 116, 21762–21770.
- [38] T. X. Wu, T. Lin, J. C. Zhao, H. Hidaka, N. Serpone, *Environ. Sci. Technol.*, **1999**, 33, 1379–1387.
- [39] M. M. Castellanos, D. Reyman, C. Sieiro, P. Calle, *Ultrason. Sonochem.*, **2001**, 8, 17–22.
- [40] J. Dillon, E. R. Gaillard, P. Bilski, C. F. Chignell, K. J. Reszka, *Photochem. Photobiol.*, **1996**, 63, 680–685.